Nanofluid Droplets Drying on Structured Surfaces and Evaporative Self-assembly

3 Nanofluid Droplets Drying on Structured Surfaces and Evaporative Self-Assembly

Veronika Kubyshkina[1], Daniel Orejon[1], Khellil Sefiane[1*]

[1]University of Edinburgh, School of Engineering, Kings Buildings, Mayfield Road, Edinburgh, EH9 3JL, UK

*Corresponding Author: k.sefiane@ed.ac.uk

ABSTRACT

Driven by growing applications involving drops interaction with solids and undergoing phase change, the topic of wetting and evaporation/drying of drops on textured surfaces has been subject to extensive recent research. In this chapter we present the results combining the evaporation of sessile droplets laden with nanoparticles and/on textured surfaces. The results demonstrate that the size, shape and spacing of textures dictate the initial shape of both pure and nanoparticle-laden low surface tension fluid drops. Circular, square, rectangular as well octagonal shapes are observed correspondingly. The drying of nanofluid drops on these textured surfaces are studied to elucidate the deposition of nanoparticles and how they are affected by the textures and the initial shape. Particles deposition following dryout is found to be enhanced near the corners where curvature is greatest. Furthermore at a high nanofluid concentration, we observe self-assembly of particles into highly ordered intricate structures deposited at the centre of the droplet.

3. 1 Introduction

Recent trends in nanotechnology, miniaturisation and intensification of processes has led to an increasing interest in liquid drops and their interactions with solids. This interest is driven by some specific applications such as inkjet printing, polymer-based LED displays, biomicroarrays, self-cleaning surfaces, etc.[1-3]. Advances on this topic allow researchers and industry to engineer surfaces with bespoke topographical and chemical characteristics. This is made possible by exploring the intricacies of the wetting phenomenon, leading to improved control of solid-liquid interactions. Modifying surface characteristics as a strategy to tune wettability enables a wide range of behaviours to be explored, ranging from complete liquid spreading on hydrophilic surfaces[4], to balled pearl drops in a non-wetting situation on superhydrophobic textured surfaces[5]. These behaviours as well as each wetting state are desirable for specific purposes in a variety of applications [6-8].

The attractive potential of tunable surface characteristics has stimulated significant research activity to extend our capacity to control droplets [9-12]. By combining micro-scale surface science with engineered surfaces, new strategies have emerged allowing manipulation and control of solid-liquid interactions. Notably, anisotropic surface texturing shows great potential for sophisticated directional wettability and adhesion [13-15]. Further, anisotropic non-wetting behaviour includes directional droplet transportation and roll-off of droplets from surfaces [16-20]. This could bring the aim of developing practical self-cleaning surfaces a step closer. Li et al. demonstrated the transition of wetting shapes of drops by adjusting topological surface features [21]. Asymmetrical droplet spreading and imbibition, through surface anisotropy, has also been widely investigated. Water droplets with 3, 4 and 6-fold symmetry have resulted from the anisotropy effect of the lattice arrangement of surface microstructures and their respective geometrical parameters [22].

A major advantage of tuning liquid behaviour on textured surfaces is the ability to generate non-spherical geometries. This would be useful for high-resolution liquid-based printing applications such as DNA sequencing and metal printing [23-24]. Desireable droplet geometries are achieved by implementing decorated surfaces with various microstructures. This manifests in a variety of polygonal shapes for both sessile drops and liquid films. Square, rectangular, hexagonal, octagonal and dodecagonal droplet footprints were induced by tuning the microstructure pillar density of intrinsically hydrophobic decorated surfaces[25]. This was exploited later to simulate the evolution of the periphery of the droplet, demonstrating the transformation of a polygonal droplet to a square one through contact line zipping [26]. Courbin et al., on the other hand, harnessed the imbibition actions of many liquid mixtures, obtaining different polygonal shapes of thin-liquid films via hydrophilic microstructure configurations [27-28]. The range of droplet profiles achieved was recently extended by including complex droplet compositions, *i.e.* liquid mixtures, surfactant and saline solutions, and/or suspensions. In recent studies, it is found that the wetting region could be controlled by altering the water-ethanol ratio on substrates with micropyramid cavities [29]. Ethanol concentration is found to dictate the transition from an octagon to a rectangle foot print. Saline droplets have also been investigated by varying concentrations of potassium chloride (KCl) in water [30]. Wetting shapes evolved from an octagon to a deformed rectangle with an increase in salt concentration on micropyramid patterned surfaces. Surfactants concentration influencing the droplet wetting shapes on textured surfaces also showed similar change in the droplet footpring or wetting shape depending on the initial concentration [31-32]. Beyond the initial shapes and their dependence on structured surface patterns, solution concentration and surfactants, wetting transitions are also observed as evaporation

proceeds. Indeed, the droplet profile transition ts from octagon to square, and from square to rectangle, was observed during the drying process [31-32]. Additionally, the ability to maintain a uniform droplet profile throughout the whole evaporation process was achieved for octagonal droplets [31-32]. Most of the studies show that surface chemistry and topography, as well as the intrinsic contact angle of the fluid, govern the wetting dynamics and droplet shape.

While the specifics of surface chemistry and topography defining the form of the wetting droplet have mostly been understood, particle deposition patterns of non-spherical droplets are still mostly unexplored. Many promising applications, where the capacity to reliably produce well-defined particulate deposits is of paramount importance for pattern-particle assembly, for example, in high-performance optical devices and sensors, would benefit from mastery of such phenomena[33-34]. It is well established that for circular and symetrical evaporating drops, particulate matter is deposited in a ring-like manner [35]. For non-circular geometries, understanding how to predict and monitor the spatial distribution of particle deposits, both accurately and effectively is a challenge still under investigation by researchers. The rich morphologies of the drying patterns are intertwined with parameters such as particle concentration, particle size, fluid composition and surface characteristics [36-39].

Studies reporting the creation of uniform deposits by manipulating the shape of the particulate matter are promising [40-41]. Choi et al. used the coffee ring effect to generate 3D micro and nanoparticle patterns using evaporation-driven self-assembly [42]. The control over deposition patterns has been achieved by creating low-adhesion superhydrophobic substrates. This showed a variety of shapes and sizes of superhydrophilic regions, and creating deposit shapes such as triangles, rectangles and ellipses [43]. Sáenz et al. integrated both experimental and theoretical approaches

for the study of evaporation kinetics and non-spherical drop deposition patterns [44], and concluded that higher curvature regions on the contact line induced greater evaporative flux resulting in non-uniform deposition patterns on the high curvature regions of the droplet periphery. Another notable study used bacteria-containing droplets to analyse the spatial distribution of deposits on micropatterned substrates[45]. More recently, Park et al. have demonstrated the ability to produce hexagonal deposits on circular micropillars utilizing colloidal suspensions of microsize particles [46]. Despite growing interest in this area, there is still a lack of understanding of the factors and mechanisms affecting the complex drying patterns of droplets containing suspensions. In some particular cases, capitalizing on surface manufacturing techniques and customized environment combinations, identification and control of particle ordering within surface structures can be achieved. Although some attention has been paid to changes in surface chemistry and topography, the emphasis has been on rudimentary surface patterning or wettability where droplets typically adopt a spherical cap geometry[46-51]. However, in the case of pure liquid droplets, flow patterns are affected by the droplet shape deviation from spherical-cap induced by the surface asperity (i.e. the sharp edge effect) [52-55]. This surface parameter may therefore be expected to alter the transport of suspended particles into solutions, adding potential deposition patterns of particle-loaded droplets to the current knowledge base.

On ideal smooth substrates, different nanoparticle deposition patterns can be realized depending on the interplay of the mechanisms takin place during drying of nanofluid droplets. The surfaces can be tailored via the wettability of the solid surface[36,37] the nature of the fluid such as pure fluids or mixtures with additives[31,32] or the pH of the solution, the ambient composition, system temperature, external forces applied, amongst others. In addition, particle concentration[36,37], shape[40], size[56], and their

wettability play a paramount role in the dynamics of droplet drying and the ordering and thickness of the deposition patterns. Starting from the coffee ring stain proposed by R. Deegan et al.[35] more than two decades ago, where particles mainly deposit at the triple contact line of a colloidal droplet evaporating in the Constant Contact Radius (CCR) mode (Figure 1a)[35], to concentric multi-rings patterns following stick-slip evaporation on low contact angle hysteresis substrates (Figure 1b)[57], to the suppression of the coffee-ring stain via asymmetric particles (Figure 1c)[40], and/or to the particle size classification during coffee ring formation (Figure 1d)[56], the wide, complex and colourful plethora of the deposits is further highlighted.

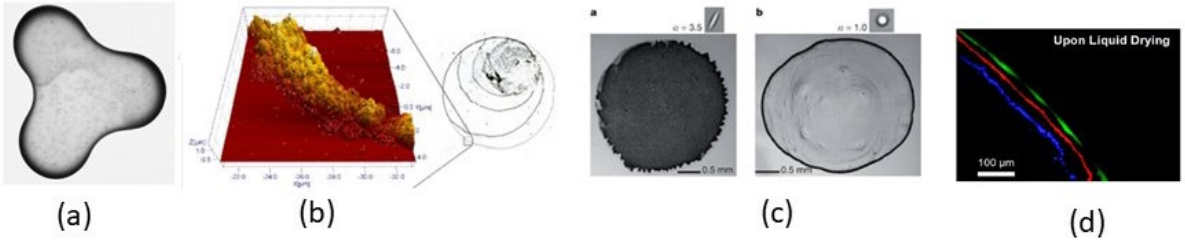

Figure 1 – (a) Coffee ring stain from Deegan et al.[35], (b) nanoparticle deposits in a concentric multi-ring fashion following stick-slip evaporation from Askounis et al. [57], (c) the suppression of the coffee-ring stain via asymmetric particles from Yunker et al.[40] (d) particle size classification or nanocrhomantography driven by the coffee ring effect from Wong et al.[56].

In this chapter two emerging fields are combined by researching the drying patterns of particle-laden droplets with complex wetting morphologies. In order to achieve this, we analyse the wetting footprints of pure liquids, and in particular the deposits left after the drying of aluminium oxide-ethanol (Al_2O_3-ethanol) nanofluid droplets of various concentrations. By integrating fluid composition and surface patterning, we demonstrate the ability to create well-defined droplet shapes and retain the desired profile during the drying process. Attention is also paid to the role of surface

topography in the selection of the shape of the droplets, namely the pillar density of the array and the shape of the micropillars. We further analyse the specifics of the surface design in relation to the deposition patterns left by the evaporated Al_2O_3-ethanol nanofluid droplets of Al_2O_3. Finally, we take a closer look at the localized deposition of particles at the microscale and assess the distribution of particles on surface microstructures, visualizing the assembly of nanoparticles at the contact line as well as at the centre after complete evaporation.

3. 2 Wetting and Evaporation of Nanofluids on Textured Surfaces

Pure liquid droplets comprised of distilled water and pure ethanol are presented in a first instance (Fisher Scientific) and nanofluid suspensions (Sigma Aldrich) secondly. Nanofluid suspensions were prepared using ethanol as the base liquid, and aluminium oxide nanopowder, Al_2O_3, with a particle size of *ca.* 50 nm (Sigma Aldrich). The solutions were prepared with concentrations of 0.01%, 0.05% and 0.1% wt. Al_2O_3-ethanol. The resulting nanoparticle liquid suspensions were sonicated for 2 hours initially, and for 30 minutes prior to each subsequent use to ensure thorough dispersion. Silicon substrates were decorated with various micropillar geometries, arranged in a square lattice and coated in hydrophobic perfluorodecyltrichlorosilane (FDTS) through vapour deposition. On smooth FDTS coated surfaces, the intrinsic contact angle for water is 112° ± 3°, whilst the corresponding value for ethanol is 60° ± 3°. The substrates were fabricated using photolithography and deep reactive ion etching (DRIE) techniques in the Scottish Microelectronics Centre (SMC) at the University of Edinburgh[16,17,58]. The geometric parameters of the micropillars are characterised by the shape, height (*h*), lateral dimensions (*d*) and edge-to-edge spacing (*s*) (*Figure 2(a)*). Whilst the height and the lateral dimensions of the pillars were kept constant (*h* = 10 +/- 2 μm and *d* = 10 μm), the shape and the spacing were

varied, giving a total of 16 surface configurations. The different micropillar shapes are visualised in *Figure 2(b)*: circular, square, star-shaped (6-point) and triangular pillars. The spacing (*s*) was varied for all pillar geometries (5, 10, 20 and 40 μm), which allowed for systematic control of surface wetting for the low surface tension fluid. The surfaces were cleaned prior to use with distilled water and dried using compressed nitrogen to remove any particulates.

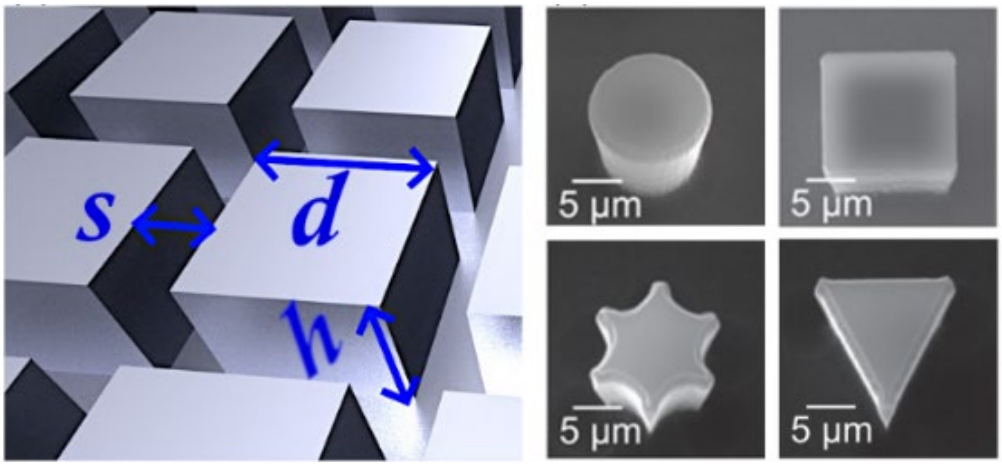

(a) **(b)**

Figure 2: (a) Schematic of an array of square pillars, with defined microscale pillar parameters: height (*h*), lateral dimensions (*d*) and edge-to-edge spacing (*s*). (b) Scanning electron microscope (SEM) images of the micropillar islands from the top, showing the different pillar geometries of lateral dimension of 10 μm: circle, square, star-shaped and triangle. Scale bar is 5 μm[59].

Droplets, of the same initial volume of 5 μl, were manually deposited on the microstructured substrates using a glass microsyringe (Hamilton). The experiments were carried out at ambient conditions (21 ± 2 °C, 46 ± 10% relative humidity, and atmospheric pressure) and repeated at least three times for each liquid/surface configuration. The profile of the deposits were visualised through a visualised through a top-down optical inspection camera (xiQ MQ013CG-ON, Ximea, Germany) with a

Nikon 105mm f/2.8 lens (AF Micro Nikkor, Nikon, Japan). Droplets were illuminated by an LCD cold light source (KL 1500, Schott, Germany). Further visualisation of the nanoparticle deposits left on the substrate after complete evaporation was conducted using an inspection microscope (DM12000 M, Leica Microsystems, Germany).The microscope was adjusted to capture the profile of the wetting area deposits, in addition to focusing on the local, microscale morphology of Al_2O_3 deposits at the contact line and droplet centre. Deposit distribution was captured both at the top of the pillars (*i.e.* the roughness level), as well as the in the space between the pillars (*i.e.* base level)[59].

3.3 Pure fluid and nanofluid droplet wetting on micro-structured surfaces

Microstructured surfaces have gained much attention in the past decades due to their potential to induce different wetting behaviours. One such discovery, recently, has been the ability to create various droplet shapes[25,31] which eventually will impact droplets evaporative behaviour, internal flows and the patterns and distribution of the drying deposits. Hence, in this chapter we introduce and discuss the research progress on wetting and drying of colloidal droplets on textured surfaces, patterned with different asperities[59]. Specifically, the relationship between the initial wetting profile and the specifics of surface topography: size and shape of the pillars and spacing between them, as well as , as well as the concentration of the nanofluid suspensions, are examined .

Although the primary interest lies in the wetting profile of nanoparticle-laden suspensions on textured surfaces of varying geometrical parameters, the wetting and non-wetting behaviour of pure liquids under the same conditions are firstly introduced to allow a comparison towards interpreting the distribution of the deposits. We highlight

in particular how changes in surface topography – the size, the shape of the pillars and the distance between pillars – affect the initial wetting or non-wetting behaviours for a low and a surface tension fluids, *i.e.*, ethanol and water. Figure 3 displays an overview of the droplet footprint, *i.e.*, snapshots looking from the top, for both pure water and pure ethanol, on microstructured surfaces of circular, square, star-shaped and triangular pillars with increasing spacing (5, 10, 20 and 40 μm), establishing a point of reference for the nanofluid droplets wetting behaviour which will be discussed later.

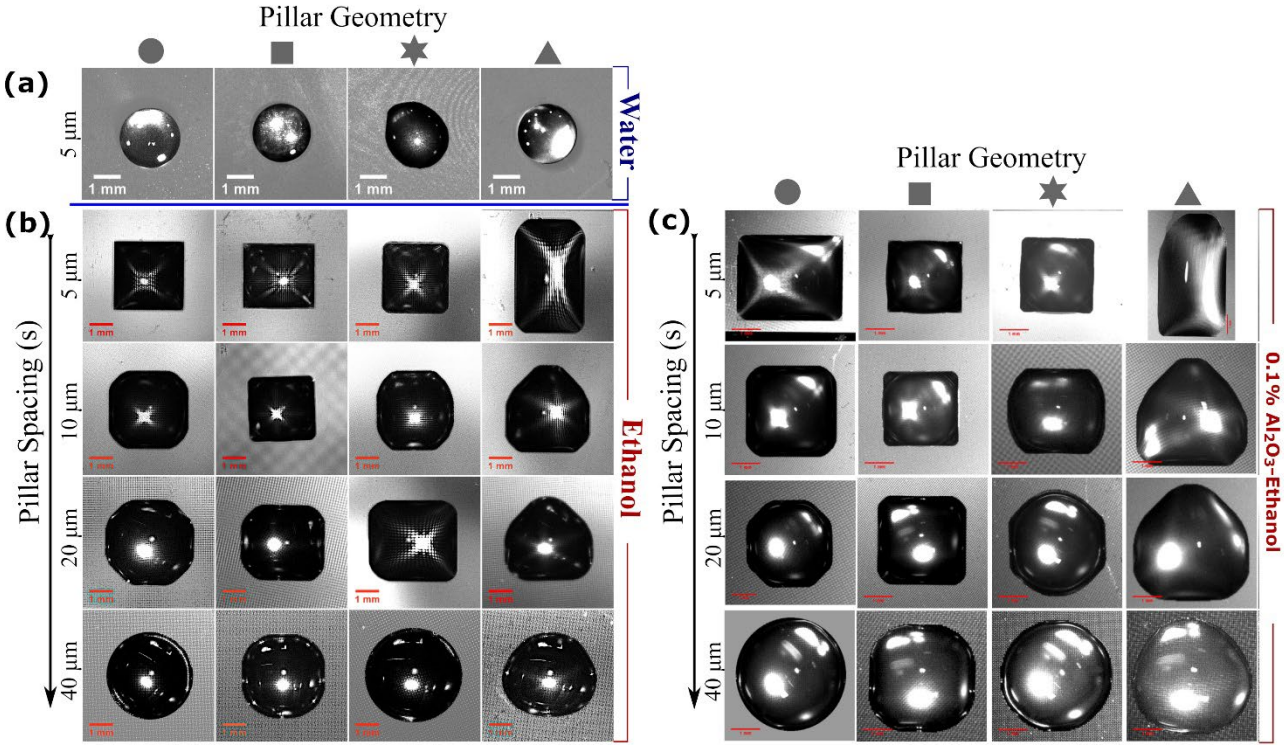

Fig. 3 Snapshots looking from the top of the initial droplet wetting profile on substrates with circular, square, star-shaped and triangular pillars (left to right). For (a) pure water droplets on substrates with different pillar geometries, all with a spacing of 5 μm; and (b) pure ethanol and (c) 0.1% Al_2O_3-ethanol nanofluid droplets on substrates with different pillar geometries and increasing pillar

spacing (*s* = 5 µm, 10 µm, 20 µm, 40 µm). Scale bar is 1 mm. Reprinted with permission from[59].

To note first here, pure water droplets (Figure 3(a)) display the expected Cassie-Baxter non-wetting behaviour, with a high contact angle, forming a spherical cap. This can be explained by the combined effect of the high surface tension of water, the low surface tension of the surface structures as a consequence of the intrinsic hydrophobicity of the coating and the presence of air entrapped between the droplet and the structures, which is consistent with the literature[8,60]. For pure water, the droplet footprint remains unaltered independently of the shape of the pillars underneath the droplet as shown in Figure 3(a) for the short pillar spacing (s = 5 µm). We note here that increasing the spacing between the structures on circular, squared or striated shaped microstructures on an intrinsically hydrophobic configuration does not alter considerably the spherical cap behaviour of the droplets resting in the Cassie-Baxter state. However, the interesting behaviour arises for low surface tension fluids, which display small intrinsic contact angle on a hydrophobic smooth and pillared configurations. For the pure ethanol case, droplets adopt a variety of droplet profiles as represented in Figure 3(b). At the higher end of pillar spacing (*s* = 40 µm), the contact line profile of ethanol droplets displays a symmetric circular shape in the wetting regime , which can be associated with the well-known spherical cap geometry. As the spacing is reduced however, the behaviour begins to diverge from a simple spherical cap; circular, square and star-shaped pillars resulting in polygonal and/or octagonal droplet peripheries at medium-range spacing (*s* = 10 and 20 µm), and quadratic peripheries at the lowest spacing (*s* = 5 µm). This behaviour is consistent with observations by Raj et al.[42], who report a transformation of the droplet wetting

area with increasing pillar density from an octagon to a square[42]. A different behaviour is observed on droplets placed on surfaces decorated with triangular pillars though, whom display an irregular polygonal shape with a loss of the contact line's axial symmetry. Here, when *s* = 10 and 20 μm, the front of the droplet approximates the shape of a triangle along the direction of the pillars, while at lower spacing of *s* = 5 μm an elongated rectangular profile was observed. This distinctive behaviour is attributed to the anisotropy of triangular pillars retarding the flow through their blunt ends, resulting in uni-directional liquid spreading, when compared to the symmetric regular shapes in the case of circular, square and star-shaped microstructures [15, 52-53]. Unidirectional droplet spreading as a consequence of the anisotropy of the surface structures was firstly reported by Chu et al.[13].

From Figure 3, the most emphatic effects on the contact line profile were caused by structure spacing, whilst pillar shape variation led to comparatively subtle geometrical differences. The diversity in behaviour displayed across surfaces warrants further attention into the subsequent evaporation behaviour and the final distribution of the deposits. The different geometrical shapes other than spherical cap in turn influences the local azimuthal curvature near the contact line being highest for example in sharp corners, with the consequent expected higher evaporation fluxin the case of non-symmetrical droplets [44]. One would expect therefore that when adding nano-particles to said droplets, a distinct variation in the deposits left in each area, in line with the difference in local evaporation rates.

Having established through pure fluids droplet analysis the above foundations for wetting behaviour, we turn our focus to the wetting and footprint of nano-particle infused liquids resting on the same surfaces and under the same conditions. Given the relatively minor variations in configurations seen for water droplets, we instead

choose to use only pure ethanol as our base for the suspensions. Although three different concentrations of dispersed aluminium oxide (Al_2O_3) nanoparticles in ethanol (0.01 wt.%, 0.05 wt.% and 0.1 wt.% wt. Al_2O_3-ethanol) are considered in this Section, to establish the role on droplet shape it behoves to consider primarily the highest of these, as it is furthest in composition from pure ethanol. Hence the droplet wetting morphologies/footprints for 0.1% wt. Al_2O_3–ethanol on micro-structured surfaces of circular, square, star and triangular shaped pillars with increasing spacing s = 5, 10, 20 and 40 μm are presented in Figure 3(c). Even at this concentration (0.1% wt. Al_2O_3–ethanol), the droplet shape is not significantly affected by the addition of nano-particles. At the higher end of pillar spacing (s = 40 μm) and similarly to pure ethanol, 0.1wt. % Al_2O_3-ethanol droplets display a circular footprint ascribed to a spherical cap profile. As the spacing is decreased (s = 10, 20 μm) the droplet shape diverges from that of simple spherical cap resulting in polygonal, octagonal and quadratic symmetric droplet peripheries on circular, square and star-shaped microscturctures, while irregular polygonal shapes with a loss of the contact line's axial symmetry on triangular one. The similar droplet wetting footprints for pure ethanol and 0.1% Al_2O_3-ethanol are then demonstrated when comparing Figure 3(b) and Figure 3(c). This is perhaps to be expected, given the minimal effect that the low concentration of nanoparticles utilised has on droplet surface tension [38, 64].

To provide some quantification on the anisotropy of the wetting droplets, the ratio length L (as the lager measured axis) to width W (as the shorter or transversal to L measured axis) L/W ; and the circularity C extracted from ImageJ, are presented in Table 1. A L/W ratio of approximate 1 signifies the symmetry of the droplet footprint either circular or in a polygonal fashion while a C equals 1 signifies a perfect circle or sphere. Since both pure ethanol (Figure 3(b)) and 0.1 wt.% Al_2O_3-ethanol nanofluid

(Figure 3(c)) droplets display a rather similar geometry and shape of the wetting footprint, for simplicity Table 1 includes the quantification solely for the nanofluid case. When comparing the ratio *L*/*W*, the greatest of the deviations is attained for the presence of asymmetric triangle microstructures and for the shortest of the spacing (*s* =5 μm), which induce uni-directional asymmetric liquid spreading and the elongated rectangular droplet footprint reported[13]. While rather uniform *L*/*W* of approximately 1 exemplifies the symmetry of the spreading in the main axis directions for symmetric pillared shapes (circular, square and star-shaped microstructures) as evidenced from Figure 3(b) and Figure 3(c). In addition to the presence of symmetries or asymmetries in the directions of the main axis, the shape/footprint of the droplets tends to deviate from spherical/circular as the spacing between structures is decreased. On all circular, square or star-shape microstructure shapes, completely round droplets *C* = 1 are reported only for *s* = 40 μm, while distorted symmetric polygonal and/or octagonal shapes deviating from spherical cap are found on *s* = 20 μm and or *s* = 10 μm with *C* = 0.8 to 0.9 and symmetric squares on s = 5 μm with *C* <0.8.

Table 1 Length (*L*) to width (*W*) ratio *L*/*W* and circularity (*C*) of the droplets for the initial wetting profile of 0.1% Al_2O_3–ethanol nanofluid on substrates with circular, square, star and triangular shaped pillars and different spacing. Values are extracted from Figure 3(b).

Pillar spacing (μm)	Circle		Square		Star		Triangle	
	L/*W*	*C* (-)	*L*/*W*	*C* (-)	*L*/*W*	*C* (-)	*L*/*W*	*C* (-)
5	1.02	0.763	1.04	0.756	1.02	0.795	1.81	0.794
10	1.00	0.866	1.02	0.813	1.16	0.894	1.03	0.884
20	1.01	0.915	1.00	0.875	1.09	0.910	1.01	0.916
40	1.03	0.978	1.01	0.930	1.00	0.983	1.04	0.951

3.4 Macroscale Deposits Morphology Left by Evaporating Nanofluid Droplets

To illustrate the distribution and morphology of the deposits, an overview of the overall deposition morphology of Al_2O_3 nanoparticles after the drying of 0.05 wt.% Al_2O_3-ethanol droplets on surfaces exhibiting various topographical features is presented. Different micropillar geometries such as square, circular, star and triangular shaped micro-structures, with varying the lateral dimension d = 5, 10, 20 and 40 μm and several pillar-to-pillar spacing s = 5, 10, 20, 40, 80, 160, 320 μm, are introduced in Figure 4.

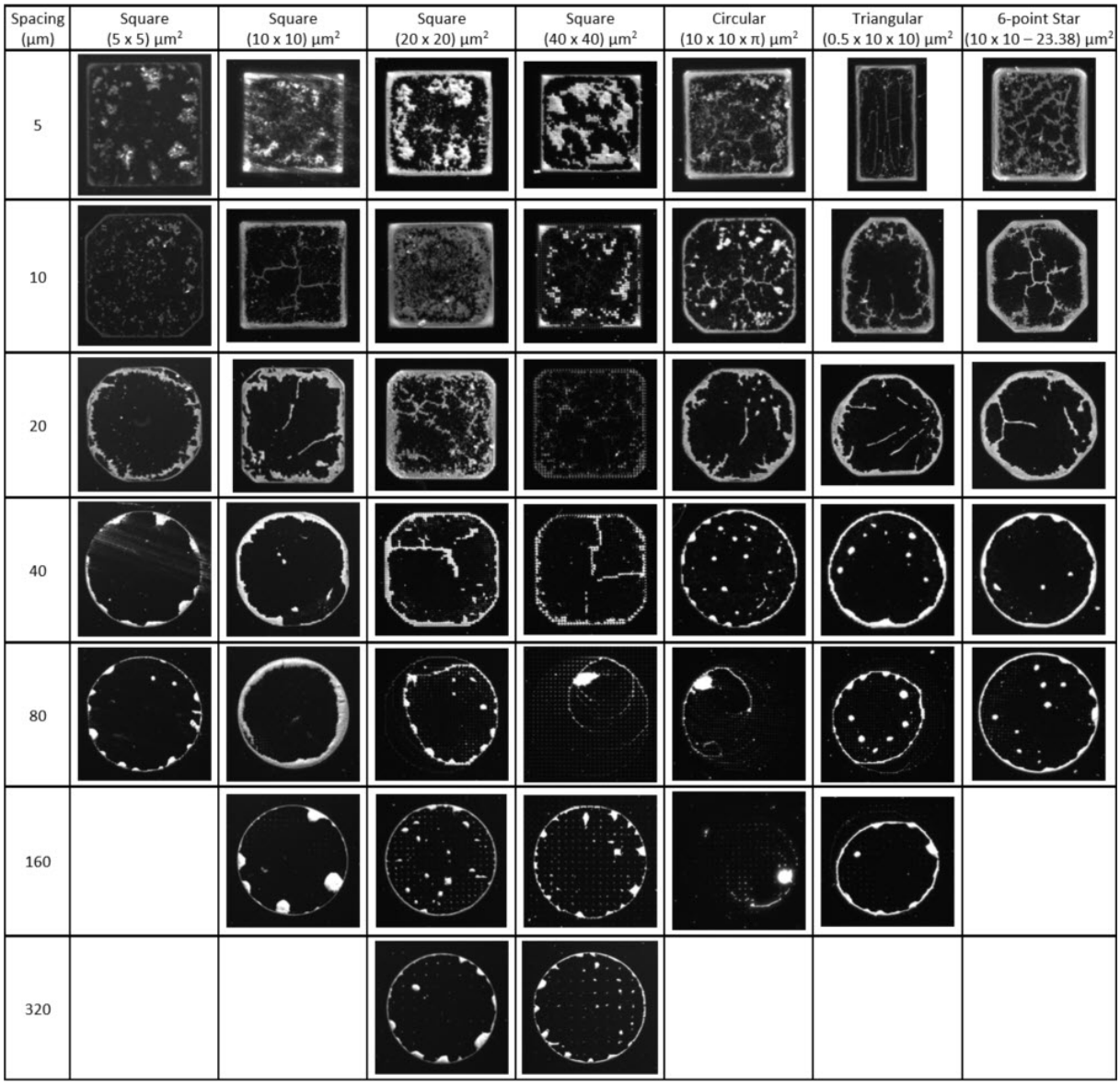

Fig. 4 Optical microscope images of Al_2O_3 nanoparticle deposits after evaporation of 0.05 wt.% Al_2O_3-ethanol droplets on square (with different the lateral dimension *d* = 5 to 40 μm), circular, triangular and star shaped pillars for different pillar spacings *s* = 5, 10, 20, 40, 80, 160, 320 μm.

From Figure 4, the symmetry of the polygonal, octagonal or quadratic shapes left by the deposits for all pillared configurations (except for anisotropic triangular microstructures with s < 40 μm) is evident. For the wide range of configurations

exemplified, the shape of regulary symmetric microstructures exerts a minimal effect on the main shape and distribution of the deposits while it is the structure spacing what dictates the main differences on the geometric shapes of the deposits. For the shortest of the spacing (s = 5 μm) deposits displaying a quadratic profile are reported independently of the shape (except for triangular pillars) and the lateral dimension of the microstructures. As the spacing is increased the main deposits shape transitions from square to polygonal and/or octagonal (s ≥ 10 μm) and then to a circular shape for larger spacing (s ≥ 40 μm). When looking into the same micropillar shape, i.e., squared micropillars, the same qualitative behaviour is observed, although the shape transitions of the deposits from squared to octagonal and to circular occur at different spacing between the structures. For squared microstructures with lateral dimension d ≥ 10 μm, the squared shape of the deposits is retained even for s = 10 μm while the circular profile of the deposits is only attained for s > 80 μm. The greatest notable differences are found on regular anisotropic triangle microstructures where the shape of the deposits transitions: from rectangle to square with a trapezoid atop, to an asymmetric circular profile with a triangle atop, to a circular profile once the spacing between pillars is large enough (s ≥ 80 μm). The shape of the deposits presented in Figure 4 are in close agreement with the wetting shapes earlier reported in Figure 3(b)&(c).

Besides the effect of structure, the concentration of the nanofluids also play an important role in the distribution of the deposits and the patterns left upon nanofluid droplet evaporation. A closer look at the distribution of the deposits on square micropillars and s = 10 μm and on trriangluar micropillars and s = 20 μm for different nanofluid concentrations: 0.01 wt.% Al_2O_3-ethanol, 0.05 wt.% Al_2O_3-ethanol and 0.1 wt.% Al_2O_3-ethanol, are included in Figure 5.

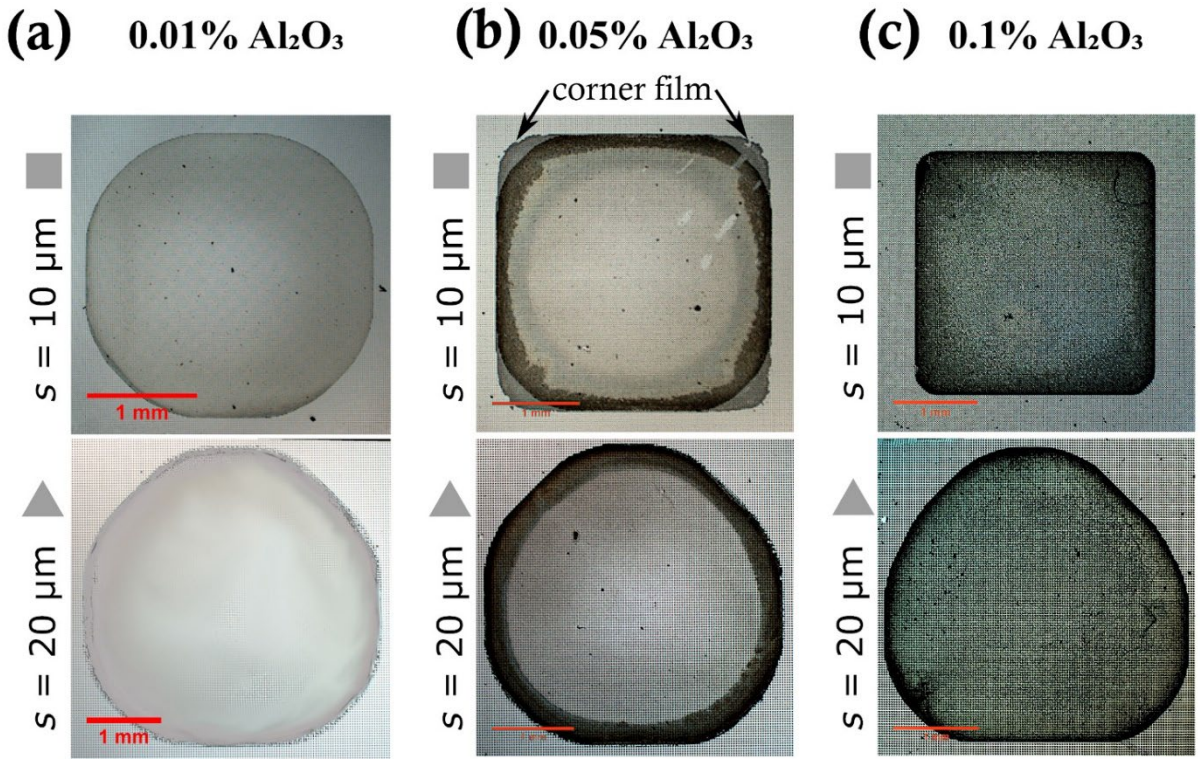

Figure 5 Optical microscope snapshots of Al_2O_3 nanoparticle deposits on (top row) squared pillars and *s* = 10 µm and (bottom row) triangular pillars and *s* = 20 µm after (a) 0.01 wt.% Al_2O_3-ethanol; (b) 0.05 wt.% Al_2O_3-ethanol and (c) 0.1 wt.% Al_2O_3-ethanol, nanofluid droplet evaporation. Scale bar is 1 mm. Reprinted with permission from[59].

The macroscopic shape adopted by the wetting droplets is independent of nanoparticle concentration and only function of the shape and spacing of the decorating structures as demonstrated in Figure 3 and Figure 4. To note is the resemblance of the deposition patterns in Figure 4 and 5 to the droplet wetting footprints introduced in Figure 3(c). The more circular or polygonal of the droplet wetting footprint dictates then the macroscopic shape and contour of the deposits at the triple contact line and/or within the droplet. For the lowest of the concentrations 0.01 wt.% Al_2O_3-ethanol, faint patterns with a slightly more defined ring-shape of the

contact line deposits are inferred from Figure 4(a). At the intermediate concentration of 0.05 wt.% Al_2O_3-ethanol, coffee-ring patterns with a more pronounced and thicker ring of the deposits is found at the contact line. For short pillar spacing (*s* = 5 μm and 10 μm) the particle density at the droplet periphery is not homogeneous presenting a rather irregular coffee-ring deposition pattern fashion as in Figure 5(b). The distribution and irregularity of the deposits are a consequence of the different droplet curvature along the contact line prompting preferential evaporation at the corners[44]. Further, in the case of 10 μm spacing on square micropillars, there is clear lighter particle when moving outwards from the contact line (arrows in Figure 5(b)), which is associated with the presence of an extended film in between the structures. Additionally, the particle deposition at the contact line is more salient and more uniform as the droplet circularity increases, i.e., spacing between pillars increases, causing a more uniform radial outward capillary flow ensuring the same flow of particles towards the contact line irrespective of the droplet azimuthal direction[20]. At the highest of the concentrations presented 0.1 wt.% Al_2O_3-ethanol, the presence of the deposits at the contact line is distinguishable; however such accumulation at the contact line is less prominent than for the intermediate and low concentration cases; and particles do accumulate and deposit at the centre of the droplet making the ring-centre boundary less obvious (Figure 5(c)). At the highest of the concentrations, i.e., ten-fold when compared to lowest concentration case, the particle-particle interaction incurs in the self-assembly and/or agglomeration partially hindering the particle motion towards the droplet periphery[61,62]. The expected lower outwards particle velocity and faster sedimentation of bigger sized particles coupled with the fast evaporation of ethanol does not allow sufficient time for the particles to reach and accumulate at the contact line, hence distributing more homogeneously along the centre of the droplet.

From macroscopic observations, it is worth confirming on the enhanced preferential accumulation of the deposits at the corners of asymmetric droplets as a consequence of the increased evaporation fluxes at those locations where the curvature of the droplet is the hightest, which is in agreement with the work of Deegan et al. and Saenz et al.[35,44]. Although the overall footprint of the deposited patterns remains unchanged, the extent of particle deposition both near the contact line and at the centre of the droplet as well as the presence of self-assembly and/or agglomerates function of the concentration deserve closer look and attention as dedicated within the next Section by looking at the deposition patterns via optical microscopy techniques.

3.5 Microscopic Depositsion Morphology Left by Evaporating Nanofluid

In what follows a closer analysis of the deposits left by the evaporated droplets at the contact line and at the droplet centre is performed to further feature the influence of the diversity of the wetted profiles observed on the microscopic morphology and distribution of the deposits. A closer inspection helps to map out the localised distribution of Al_2O_3 nanoparticles on the surface microstructures at the three-phase contact line and at the centre of the droplet. To further interpret and give account of the particle distribution, a closer look at the effect of micropillar geometry, micropillar spacing and nanofluild concentration at the different localised regions as well as the particle self-assembly is presented in the next subsections.

3.5.1 Localised Microscale Deposition: Effect of Pillars Geometry

First, we bring our attention to symmetric micropillared structures where regular wetting polygonal shapes yield symmetric distribution of the wetting droplet and the deposits profiles as introduced earlier in Figure 3 and Figure 4. Square micropillars

and circular micropillars are introduced in Figure 6(left) and Figure 6(right) so to establish the effect of pillar geometry on the localised microscale deposition. Details of particle deposition are examined at the three-phase contact line ((a) & (b)) and the centre of the droplet ((c) & (d)), on the pillar islands ((a) & (c)) as well as between pillars ((b) & (d)).

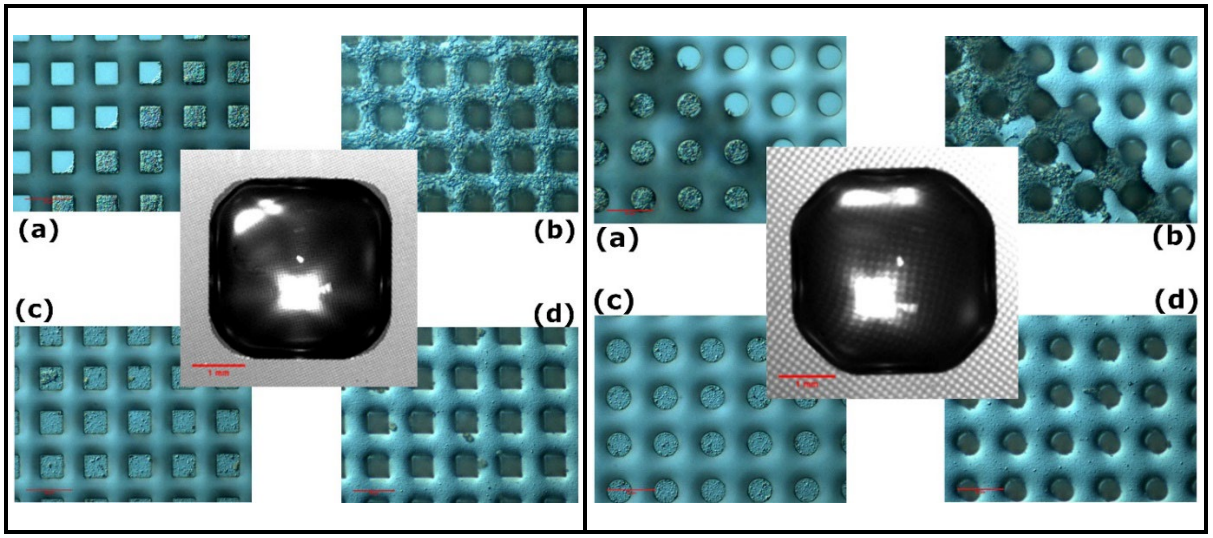

Figure 6: Nanoparticle deposition after evaporation of a 0.05 wt.% Al_2O_3–ethanol droplet solution on (left) square pillars and *s* = 10 μm and (right) circular pillars and *s* = 10 μm spacing. Optical microscopy snapshots of the nanoparticles deposition are shown for (a) top of the pillars at the contact line; (b) between pillars at the contact line; (c) top of the pillars in the centre of droplet; (d) between pillars in the centre of droplet. The initial wetting profile is shown in the middle for illustration.

We draw attention to the distribution of nanoparticles on pillar islands, as well as in the space between the pillars - denoted as roughness level and base level both at the contact line and within the droplet. Of interest is to highlight the similar distribution of the deposits independently of the geometry of the symmetric pillared structures both

at the macroscale (Figure 4) and at the microscale (Figure 6). When looking at the deposits left at the centre of the droplet, the majority of the deposits are localised on the pillars tops while less accumulation of the deposits is found between the structures as exemplified in panels (c) and (d) on both Figure 6(left) and Figure 6(right). At the contact line though, the deposits distribute consistently both on the top and between the pillars as shown in panels (a) and (b) on both Figure 6(left) and Figure 6(right). On both pillared surfaces the location of the contact line is clearly denoted as per the presence of deposits on the top of pillars adjacent to clean deposits free pillars (see panel Figure 6(left)(a) and Figure 6(right)(a)). When looking at the deposits found between structures near the contact line though, some apparent differences can be inferred when comparing squared to circular pillars decorated surfaces. In the case of circular pillars, the distribution of the deposits seems to be constrained by the location of the contact line, whereas for squared micropillars, some deposits are found when moving outwards from the contact line as seen from panel (b) on Figure 6(right) and Figure 6(left), respectively. The presence of deposits extending further away from the position of the contact line is attributed to the occurrence of an extended film as it can be inferred when looking at the corners of the droplet wetting snapshot presented in Figure 6(left) and were previously pointed out in Figure 5(b)(top). Such extended film was observed in the case of square micropillars with s = 5 μm and 10 μm while no film was observed for circular pillars with $s \geq 10$ μm.

Once established the similarities of the deposition patterns in the presence of regular symmetric microstructures, the additional effect of microstructure anisotropy on the wetting profile and hence on the distribution of the deposits deserves further focus. Next, a closer microscopic look at the deposits distribution at the contact line in the presence of anisotropic triangular microstructures (yielding asymmetric wetting

profiles and asymmetric main shape of the deposits) and in the presence of symmetric circular microstructures (yielding regular polygonal wetting shapes and main shape of the deposits to allow for comparission), is introduced. The microscopic view of the droplet periphery at the convex corners of a 0.1 wt.% Al_2O_3-ethanol nanofluid is shown in Figure 7 through two different surface configurations: circular micropillars of lateral dimensions d = 5 µm in size and spacing s = 20 µm and triangular micropillars of lateral dimensions d = 10 µm in size and spacing s = 5 µm. Microscopic observations of the deposition patterns confirm the existence of the zip-wetting system attributed to the adopted non-spherical wetting footprints on decorated surfaces [25-27].

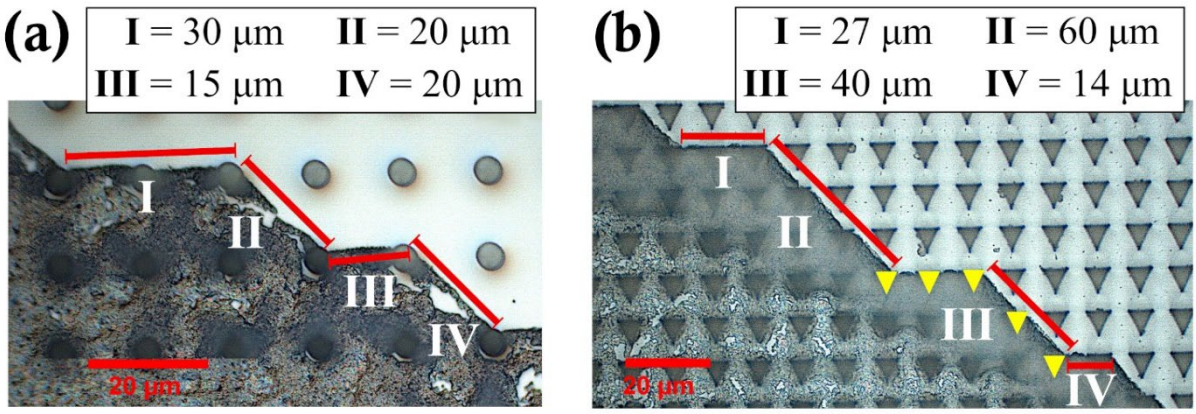

Figure 7 Optical microscope images of the deposits left by a 0.1 wt% Al_2O_3-ethanol droplet at the contact line corner on a surface patterned with (a) circular micropillars of of lateral dimensions d = 5 µm and spacing s = 20 µm and (b) triangular micropillars of lateral dimensions d = 10 µm and spacing s = 10 µm spacing. Scale bar is 20 µm. Reprinted with permission from[59].

When comparing surfaces decorated with circular (Figure 7(a)) to triangular (Figure 7(b)) pillars, there are clear variations in the length of the deposits in the orthogonal and diagonal directions. On triangular micropillared surfaces, the more elongated

wetting profile of the droplets exerts an increased pinning length along the diagonal with measured lengths between 40 μm and 60 μm as for segments II and III in Figure 7(b). This is caused by the rapid and unimpeded distribution of fluid between the posts. This result is consistent with Blow et al.'s simulations of triangular pillars, which provides a detailed description of the imbibition and pinning dynamics of anisotropic droplet activity[52-53]. In the presence of circular micropillars, the more symmetric polygonal footprints adopted and the absence of contact line preferential elongation on a predefined direction, keep the diagonal segments II and IV within 20 μm, i.e., 2 or 3 times smaller than on anisotropic triangular pillars and within the same values as the contact line lengths in the longitudinal/horizontal direction.

3.5.2 Localised Microscale Deposition: Effect of Pillar Spacing

The effect of micropillar spacing, which has a more enfatic effect on the droplet wetting profile and on the final shape of the deposits as reported earlier in Figure 3 and Figure 4, is addressed next. Circular micropillars with lateral dimension d = 10 μm and spacing s = 10 and 40 μm are presented in Figure 8(left) and Figure 8(right), respectively. Special attention is paid to the localised microscale deposition at the three-phase contact line ((a) & (b)) and the centre of the droplet ((c) & (d)) on the pillar islands ((a) & (d)) as well as between pillars ((b) & (d)) left from the evaporation of a 0.05 wt. % Al_2O_3–ethanol droplet. The wetting profile upon deposition is included for comparison.

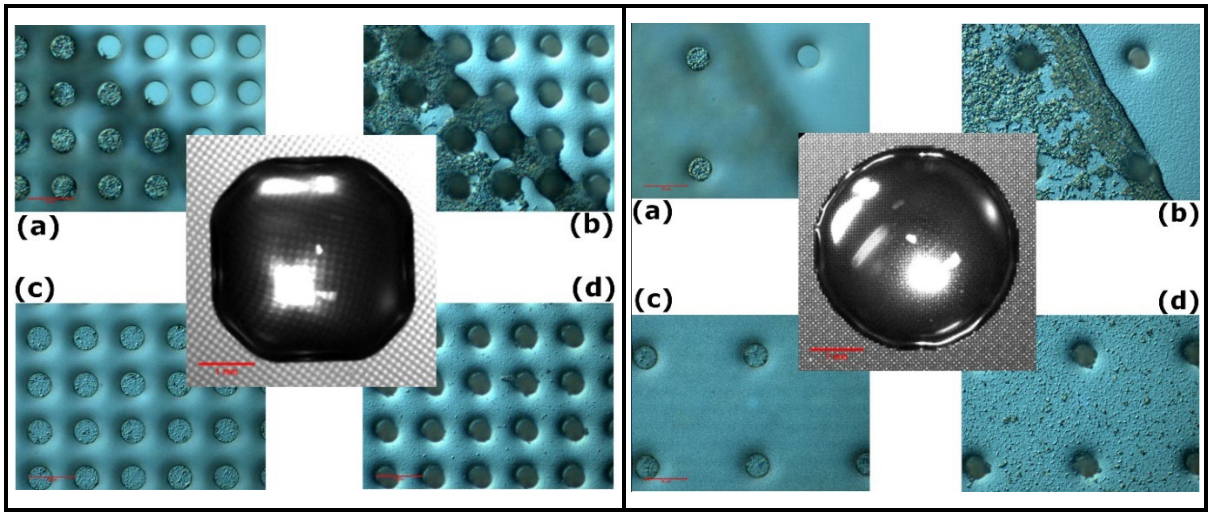

Figure 8 Nanoparticle deposition after an evaporation of a 0.05 wt. % Al_2O_3–ethanol droplet on circular micropillars for (left) *s* = 10 μm and (right) *s* = 40 μm. Optical microscopy snapshots of the nanoparticles deposition are shown for (a) top of the pillars at the contact line; (b) between pillars at the contact line; (c) top of the pillars at the centre of droplet; (d) between pillars at the centre of droplet. The initial wetting profile is shown in the middle for illustration.

When looking at nanoparticles deposition at the droplet centre, there is absence of particle deposition on both the pillars' tops and in between pillars for short micropillared spacing $s \leq 10$ μm (Figure 8(left)), while a more prominent accumulation of the deposits between pillars is noted as the pillar pitch increases $s \geq 20$ μm. Since the pillar geometry does not affect considerably the distribution of the deposits, this behaviour can be generalised to all pillar geometries, which will be further demonstrated in a subsequent section. The absence of particle accumulation at the centre of the droplet for short pillar-to-pillar spacing inducing the most emphatic droplet shape differences from spherical cap can be attributed to the non uniform radial flows taking place within the droplet as a consequence of the different from spherical cap geometry reported inducing greater evaporative flux at the corners[44]. The non-

uniformity of the radial outward flows within the droplet may enhance mixing within the droplet hence hindering the deposition of particles at the centre.

The more accumulation of particles at the droplet centre signifies, in turn, the less expected nanoparticle deposition at the contact line as per mass conservation. When looking at the pillars' tops, no major differences can be appreciated when comparing the different pillar-to-pillar spacing. Nonetheless, between pillars, the particle deposition is richer and denser and no gaps are present between deposits when decreasing the pillar spacing as for $s \leq 10$ μm where a contact line with thickness equals to the micropillar size is reported in Figure 7(left) while more fainted deposition is found in for $s = 40$ μm in Figure 7(right).

3.5.3 Localised Microscale Deposition: Effect of Nanoparticle Concentration

In this subsection, we draw the attention to the nanoparticles distribution function of the nanofluids concentration. The deposits left after evaporation of 0.01 wt.% Al_2O_3-ethanol (Figure 9(a)&(c)) and 0.1 wt.% Al_2O_3-ethanol (Figure 9(b)&(d)) at the top of pillars and between pillars at both the contact line and at the droplet centre are introduced presented and discussed next. In addition, two different pillared structures: squared pillars with lateral dimension $d = 10$ μm and spacing $s = 5$ μm spacing and star-shaped pillars with lateral dimension $d = 10$ μm and spacing $s = 20$ μm are introduced in Figure 9(a)&(b) and Figure 9(c)&(d), respectively. Since the presence of symmetric micropillar geometries was found to have a rather negligible effect on the wetting droplet footprint and on the distribution of the deposits, the two structured surfaces proposed allow for a more detailed comparison and discussion of the nanoparticle accumulation and/or self-assembly function of the nanoparticle concentration and microstructure spacing.

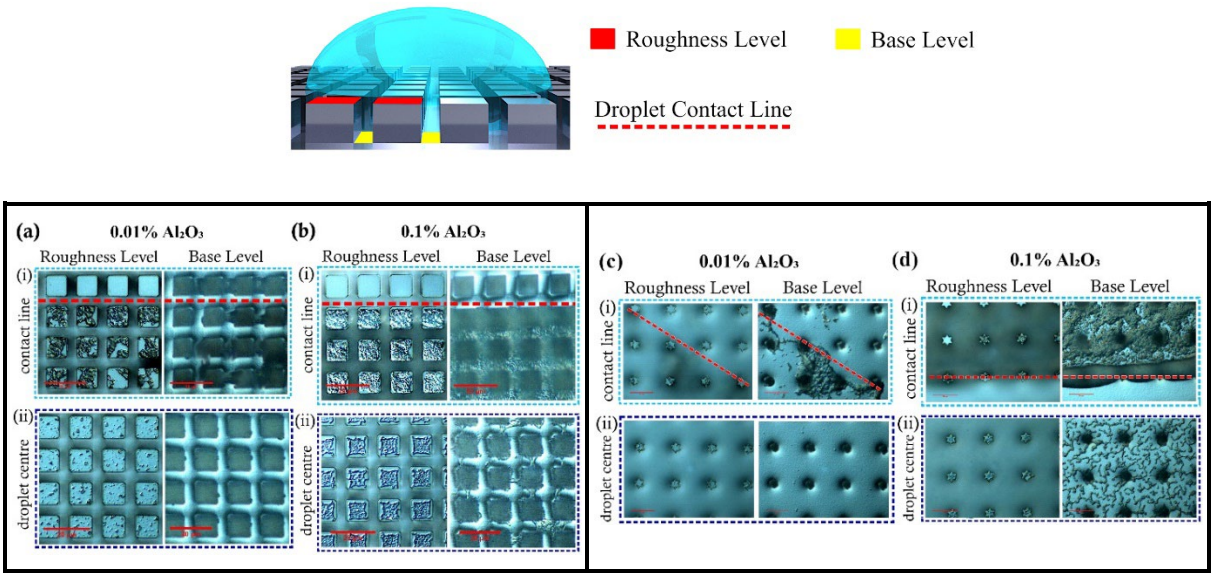

Figure 9 Optical microscopy snapshots of localised Al_2O_3 nanoparticle deposition patterns at the contact line on (left) squared micropillars with spacing *s* = 5 μm and (right) star-shaped micropillars with spacing *s* = 20 μm after (a) 0.01 wt.% Al_2O_3-ethanol and (b) 0.1 wt.% Al_2O_3-ethanol nanofluid droplet evaporation. Panels show (i) the contact line and (ii) the centre of the droplet focusing at the top of the pillars and at the base level between the pillars as represented in (top) schematic. Scale bar is 20 μm. (left) Reprinted with permission from Ref. [59].

For the lowest of the concentrations 0.01 wt.% Al_2O_3-ethanol, there is a clear absence of particle deposition at the droplet centre both at the pillars' tops and between pillars independently of the microstructure spacing as demonstrated in Figure 9(a)(ii) and Figure 9(c)(ii). When moving near the contact line, there is a greater proportion of particles accumulated as a consequence of the advective outwards flow predominant during evaporation of pinned droplets. In the case of square shaped pillars with lateral dimiension *d* 10 μm and spacing *s* = 5 μm (Figure 9(a)(i)) there is more particle deposition at the micropillars' tops while less accumulation of the deposits ensues at

the base level as a consequence of the confined space available for particle sedminetatoin between pillars. Conversely, for larger spacing on star-shaped pillars with lateral dimension *d* =10 10 μm star shaped and spacing *s* = 20 μm, the distribution of the deposits near the contact line is somewhat opposite. Greater accumulation of the deposits is found between pillars while less deposits are found at the pillars' tops with clear visible gaps as seen in Figure 9(c)(i).

At higher nanofluid concentration of 0.1 wt.% Al_2O_3-ethanol, the distribution of the deposits changes significantly when looking at the centre of the evaporated droplet. At the contact line, the deposits are denser across all levels of the surface with complete coverage of the available surface area, clearly visible when comparing Figure 9(b)&(d)(i) to Figure 9(a)&(c)(i).The pillars' tops are found coated in a deposition pattern matching that of the pillar shape, albeit with a surrounding border. The particle accumulation is more evident and uniform throughout the pillars' tops for squared shaped pillars with lateral dimiension *d* = 10 μm and spacint *s* = 5 μm (Figure 9(b)(i)) while gaps at the pillars' tops with absence of nanoparticles can be observed at the top of star-shaped pillars with lateral dimension *d* = 10 μm and spacing *s* = 20 μm (Figure 9(d)(i))Figure 9(d)(i). When looking into the effect of nanofluid concentration, the increased concentration yields the full coverage of the pillared structures when compared to lower concentrations where the top of the pillars are visible in the case of squared shaped pillars with lateral dimiension *d* = 10 μm and spacint *s* = 5 μm (Figure 9(b)(i)).

When focusing our attention to the centre of the droplet, scarce nanoparticle deoposition is found at low nanofluid concentration both at the top and between pillars (Figure 9(a)(ii) versus Figure 9(c)(ii)) evidencing that most of the nanoparticles travel

and deposit near the contact line. When increasing the nanofluid concentration, of major interest is to note the different nanoparticle accumulation and the distinctive nanoparticle self-assembly into branch-type formations found between pillars, where the quantity, length, width and intrincate of the branch-like structures are highly dependent on the spacing between the structures. The dependence of the self-assembly taking place between pillars on nanoparticle concentration and on the pillar-to-pillar spacing deserves a further section to comment on this phenonemon.

3.5.4 Localised Microscale Deposition: Nanoparticle Self-Assembly

The next section compares the different distribution and self-assembly of the deposits left at the centre after the complete evaporation of a nanofluid droplet varying in the concentration on two different micropillared substrates. Having established that the geometry of the pillars does not play a major role on the droplet wetting footprint and on the final particle distribution of the deposits; the pay a closer look at the accumulation of deposits upon evaporation of an intermediate nanofluid concentration 0.05 wt.% Al_2O_3-ethanol nanofluid droplet and high nanoflconcentration 0.1 wt.% Al_2O_3-ethanol droplets on on circular andon star-shaped pillars, respectively, with varying spacing s = 5, 10, 20, 40 μm. This allows for the thorough comparison on the nanoparticle self-assembly function of the nanofluid concentration and the pillar spacing, which is introduced in Figure 10.

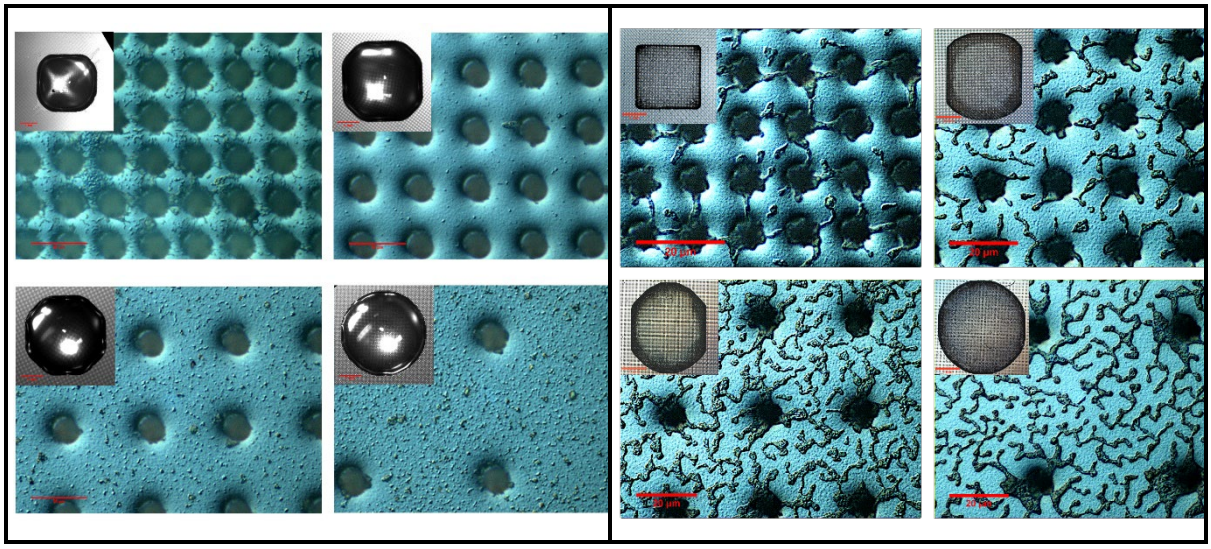

Figure 10 Optical microscopy snapshots showing the morphology and distribution of the particle depostis for (left) 0.05 wt.% Al_2O_3-ethanol nanofluid on circular micropillars with lateral dimension *d* = 10 μm and spacing *s* = 5, 10, 20 and 40 μm, and (right) 0.1 wt.% Al_2O_3 nanofluid on star micropillars with lateral dimension *d* = 10 μm and spacing *s* = 5, 10, 20 and 40 μm.. The scale bar of the optical microscopic snapshots is 20 μm. The droplet shape and deposition footprint are shown as the inserts with a scale bar of 1 mm. (right) Reprinted with permission from[59].

The more predominant highly ordered nanoparticle self-assembling is found between pillars for the highest of the concentrations 0.1 wt.% Al_2O_3-ethanol nanofluid when compared to the intermediate concentration 0.05 wt.% Al_2O_3-ethanol, i.e., when comparing Figure 10(right) to Figure 10(left). Henceforth we focus the attention of this section solely on the deposits reported for 0.1 wt.% Al_2O_3-ethanol in Figure 10(right). The fractal branched aggregates orginate at the base of the pillars, and extend radially outward increasing in the length and the complexity of the structures as the pillar-to-pillar spacing increases (Figure 10(right)). This is owed to the increase of the particle-particle and particle-fluid interactions as the nanoparticle concentration is increased

resulting in enhanced agglomeration and self-assembly[63]. The constrained geometry in the presence of short pillar-to-pillar spacing does not allow for efficient particle-particle and particle-fluid interactions when compared to larger spacing, and as a consequence shorter self-assembled agglomerates are found, while thicker and larger self-assembled chains are found at larger spacing. In addition, the lower accumulation of nanoparticles between pillars for tightly packed pillars is explained in terms of the self-assembled agglomerates not being small enough to deposit between pillars being free to move above the structures by the internal outwards flow presumabilty driving the agglomerates towards the contact line. While the longer and more intrincate self-assembled agglomerates are able to deposit between the structures in the case of larger spacings. The effect of particle concentration,pillar geometry and pillar-to-pillar spacing on the nanoparticle self-assembly and on the distribution of the deposits forming intricate patterns is here highlighted, which may be further exploited to tailor-made advanced unique surface patterns for specific technological applications.

5. Conclusions

The wetting and evaporation of droplest on structured surfaces has great potential. Structuring surfaces can help control both the shape of the wetting droplets from spherical cap to regular polygons (squares, hexagons, octagons, etc.) to non-axysimetric or elongated geometries, and therefore the evaporation kinetics of droplets. Generating specific geometries of liquid droplets by tuning surface microstrures can help achieving desireable outcomes for specific applications. The depositions of nanomaterials from drying droplets is another aspect which can be exploited in conjunction with microstructured surfaces to achieve technologies otherwise not possible. In summary we demonstrate that in the case of symmetric micropillared structures the pillar-to-pillar spacing (and not the pillar geometry and/or

the pillar lateral dimension) play a major role on the control of the droplet wetting shape and on the final distribution of the deposits near the contact line and at the centre. The nanofluid concentration was also found to play a big role about all on the morphology and the distribution of the nanoparticle patterns left at the droplet centre.

Acknowledgements

This research is funded partly through an EPSRC DTC studentship. The authors would like to thank the European Space Agency through grant ESA Contract Number 4000129506/20/NL/PG.

6. References

1. Calvert P. Inkjet printing for materials and devices. *Chemistry of materials*, 2001**,** **13**, 3299-3305.

2. de Gans B. J, Schubert, U. S., Inkjet printing of well-defined polymer dots and arrays. *Langmuir*, 2004, **20**, 7789-7793.

3. Yoshino M, Matsumura T, Umehara N, Akagami Y, Aravindan S, Ohno T. Engineering surface and development of a new DNA micro array chip. *Wear*, 2006**,** **260**, 274-286.

4. Bico J, Thiele U, Quéré D. Wetting of textured surfaces. *Colloids and Surfaces A: Physicochemical and Engineering Aspects*, 2002, **206**, 41-46.

5. Quéré D. Rough ideas on wetting. *Physica A: Statistical Mechanics and its Applications,* 2002, **313**, 32-46.

6. Zhang W, Zhu Y, Liu X, Wang D, Li J, Jiang L, Jin J. Salt-Induced Fabrication of Superhydrophilic and Underwater Superoleophobic PAA-g-PVDF Membranes for Effective Separation of Oil-in-Water Emulsions. *Angewandte Chemie International Edition,* 2014, **53**, 856-860.

7. Chu K-H, Enright R, Wang E N. Structured surfaces for enhanced pool boiling heat transfer. *Applied Physics Letters,* 2012, **100**, 241603.

8. Bico J. Pearl drops. *EPL (Europhysics Letters),* 1999, **47**, 220-226.

9. Ralf B. Self-cleaning surfaces — virtual realities. *Nature Materials,* 2003, **2**, 301.

10. Cao L, Jones A K, Sikka V K, Wu J, Gao D. Anti-icing superhydrophobic coatings. *Langmuir,* 2009, **25**, 12444.

11. Sun, Y.; Guo, Z., Recent advances of bioinspired functional materials with specific wettability: from nature and beyond nature. *Nanoscale Horizons* **2019,** *4* (1), 52-76.

12. Orejon D, Askounis A, Takata Y, Attinger D. Dropwise Condensation on Multiscale Bioinspired Metallic Surfaces with Nanofeatures. *ACS Applied Materials & Interfaces,* 2019, **11**, 24735-24750.

13. Chu K H, Xiao R, Wang E N. Uni-directional liquid spreading on asymmetric nanostructured surfaces. *Nature Materials,* 2010, **9**, 413-417.

14. Liu M, Li J, Zhou X, Li J, Feng S, Cheng Y, Wang S, Wang Z. Inhibiting Random Droplet Motion on Hot Surfaces by Engineering Symmetry-Breaking Janus-Mushroom Structure. *Advanced Materials,* 2020, **32**, 1907999.

15. Sun G, Fang Y, Cong Q, Ren L-Q. Anisotropism of the Non-Smooth Surface of Butterfly Wing. *Journal of Bionic Engineering,* 2009, **6**, 71-76.

16. Kita, Y., Mackenzie Dover, C., Askounis, A., Takata, Y., Sefiane, K. Drop mobility on superhydrophobic microstructured surfaces with wettability contrasts .Soft Matter, 2018, **14**, 9418-9424.

17. Zhao, H., Orejon, D., Mackenzie-Dover, C., Valluri, P., Shanahan, M.E.R., Sefiane, K. Droplet motion on contrasting striated surfaces. *Applied Physics Letters*, 2020, **116**, 251604.

18. Jokinen V, Sainiemi L, Franssila S. Complex Droplets on Chemically Modified Silicon Nanograss. *Advanced Materials,* 2008, **20**, 3453-3456.

19. Jokinen V, Leinikka M, Franssila S. Microstructured Surfaces for Directional Wetting. *Advanced Materials,* 2009, **21**, 4835-4838.

20. Yunusa M, Ozturk F E, Yildirim A, Tuvshindorj U, Kanik M, Bayindir M. Bio-inspired hierarchically structured polymer fibers for anisotropic non-wetting surfaces. *RSC Advances,* 2017, **7**, 15553-15560.

21. Li X, Mao L, Ma X. Dynamic behavior of water droplet impact on microtextured surfaces: the effect of geometrical parameters on anisotropic wetting and the maximum spreading diameter. *Langmuir,* 2013, **29**, 1129.

22. Vrancken R J, Blow M L, Kusumaatmaja H, Hermans K, Prenen A M, Bastiaansen C W, Broer D J, Yeomans J M. Anisotropic wetting and de-wetting of drops on substrates patterned with polygonal posts. *Soft Matter,* 2013, **9**, 674-683.

23. Barbulovic-Nad I, Lucente M, Sun Y, Zhang M, Wheeler A R, Bussmann M. Bio-Microarray Fabrication Techniques-A Review. *Critical Reviews in Biotechnology,* 2006, **26**, 237-259.

24. Park B K, Kim D, Jeong S, Moon J, Kim J S. Direct writing of copper conductive patterns by ink-jet printing. *Thin Solid Films,* 2007, **515**, 7706-7711.

25. Raj R, Adera S, Enright R, Wang E N. High-resolution liquid patterns via three-dimensional droplet shape control. *Nature Communications,* 2014, **5**, 8.

26. Kumar A, Raj R. Droplets on Microdecorated Surfaces: Evolution of the Polygonal Contact Line. *Langmuir,* 2017, **33**, 4854-4862.

27. Courbin L, Denieul E, Dressaire E, Roper M, Ajdari A, Stone H A. Imbibition by polygonal spreading on microdecorated surfaces. *Nature Materials,* 2007, **6**, 661-664.

28. Courbin L, Bird J C, Reyssat M, Stone H A. Dynamics of wetting: from inertial spreading to viscous imbibition. *Journal of Physics-Condensed Matter,* 2009, **21**, 13.

29. Feng H, Chong K S-L, Ong K-S, Duan F. Octagon to Square Wetting Area Transition of Water-Ethanol Droplets on a Micropyramid Substrate by Increasing Ethanol Concentration. *Langmuir,* 2017, **33**, 1147.

30. Zhong X, Ren, J, Lin, M, Chong K, Ong K S, Duan F. Octagonal Wetting Interface Evolution of Evaporating Saline Droplets on a Micropyramid Patterned Surface. *ACS Applied Materials & Interfaces,* 2017, **9**, 28055-28063.

31. Zhong X, Ren J H, Chong K S L, Ong K S, Duan F. Controlling Octagon-to-Square Wetting Interface Transition of Evaporating Sessile Droplet through Surfactant on Microtextured Surface. *ACS Applied Materials & Interfaces,* 2018, **10**, 11425-11429.

32. Zhong X. Ren J, Chong K S-L, Ong K-S, Duan F. Wetting Transition at a Threshold Surfactant Concentration of Evaporating Sessile Droplets on a Patterned Surface. *Langmuir,* 2019, **35**, 4509–4517.

33. Mihi A, Zhang C, Braun P V. Transfer of preformed three-dimensional photonic crystals onto dye-sensitized solar cells. *Angewandte Chemie International Edition,* 2011, **50**, 5712.

34. Xu X, Goponenko A V, Asher S A. Polymerized PolyHEMA photonic crystals: pH and ethanol sensor materials. *Journal of the American Chemical Society,* 2008, **130**, 3113.

35. Deegan R, Bakajin O, Dupont T, Huber G, Nagel S, Witten T. Capillary flow as the cause of ring stains from dried liquid drops. *Nature,* 1997, **389**, 827.

36. Sefiane K. On the Formation of Regular Patterns from Drying Droplets and Their Potential Use for Bio-Medical Applications. *Journal of Bionic Engineering,* 2010, **7**, S82-S93.

37. Orejon D, Sefiane K, Shanahan M E R. Stick-slip of evaporating droplets: substrate hydrophobicity and nanoparticle concentration. *Langmuir,* 2011, **27**, 12834.

38. Bhuiyan M, Saidur R, Amalina M, Mostafizur R, Islam A. Effect of nanoparticles concentration and their sizes on surface tension of nanofluids. *Procedia Engineering,* 2015, **105**, 431-437.

39. Choi Y, Han J, Kim C. Pattern formation in drying of particle-laden sessile drops of polymer solutions on solid substrates. *Korean Journal of Chemical Engineering,* 2011, **28**, 2130-2136.

40. Yunker P J, Still T, Lohr M A, Yodh A. Suppression of the coffee-ring effect by shape-dependent capillary interactions. *Nature,* 2011, **476**, 308.

41. Larson R G. Re-Shaping the Coffee Ring. *Angewandte Chemie International Edition,* 2012, **51**, 2546-2548.

42. Choi S, Stassi S, Pisano A P, Zohdi T I. Coffee-Ring Effect-Based Three Dimensional Patterning of Micro/Nanoparticle Assembly with a Single Droplet. *Langmuir,* 2010, **26**, 11690-11698.

43. He A, Yang H, Xue W, Sun K, Cao Y. Tunable coffee-ring effect on a superhydrophobic surface. *Optics Letters,* 2017, **42**, 3936-3939.

44. Sáenz P J, Wray A W, Che Z, Matar O K, Valluri P, Kim J, Sefiane K. Dynamics and universal scaling law in geometrically-controlled sessile drop evaporation. *Nature Communications,* 2017, **8**.

45. Susarrey-Arce A, Marin A, Massey A, Oknianska A, Díaz-Fernandez Y, Hernández-Sánchez J F, Griffiths E, Gardeniers J G E, Snoeijer J H, Lohse D, Raval R. Pattern Formation by Staphylococcus epidermidis via Droplet Evaporation on Micropillars Arrays at a Surface. *Langmuir,* 2016, **32**, 7159.

46. Park H K, Kim Y, Min H, Pang C, Weon B M. Hexagonal deposits of colloidal particles. *Physical Review E,* 2019, **100**, 022602.

47. Dicuangco M, Dash S, Weibel J A, Garimella S V. Effect of superhydrophobic surface morphology on evaporative deposition patterns. *Applied Physics Letters,* 2014, **104**, 201604.

48. Xu W, Leeladhar R, Tsai Y-T, Yang E-H, Choi C-H. Evaporative self-assembly of nanowires on superhydrophobic surfaces of nanotip latching structures. *Applied Physics Letters,* 2011, **98**, 073101.

49. Cui L, Zhang J, Zhang X, Li Y, Wang Z, Gao H, Wang T, Zhu S, Yu H, Yang B. Avoiding coffee ring structure based on hydrophobic silicon pillar arrays during single-drop evaporation. *Soft Matter,* 2012, **8**, 10448-10456.

50. Fan F, Stebe K J. Assembly of colloidal particles by evaporation on surfaces with patterned hydrophobicity. *Langmuir,* 2004, **20**, 3062-3067.

51. Marín Á G, Gelderblom H, Susarrey-Arce A, van Houselt A, Lefferts L, Gardeniers J G, Lohse D, Snoeijer J H. Building microscopic soccer balls with evaporating colloidal fakir drops. *Proceedings of the National Academy of Sciences,* 2012, **109**, 16455-16458.

52. Blow M L, Kusumaatmaja H, Yeomans J M. Imbibition through an array of triangular posts. *Journal of Physics: Condensed Matter,* 2009, **21**, 464125.

53. Blow M L, Yeomans J M. Anisotropic imbibition on surfaces patterned with polygonal posts. *Philosophical Transactions of the Royal Society A: Mathematical, Physical and Engineering Sciences,* 2011, **369**, 2519-2527.

54. Wang Z, Lin K, Zhao Y-P. The effect of sharp solid edges on the droplet wettability. *Journal of Colloid and Interface Science,* 2019, **552**, 563-571.

55. Chauvet F, Duru P, Prat M. Depinning of evaporating liquid films in square capillary tubes: Influence of corners' roundedness. *Physics of Fluids,* 2010, **22**, 112113.

56. Wong T-S, Chen T-H, Shen X, Ho C-M. Nanochromatography driven by the coffee ring effect. *Analytical chemistry,* 2011, **83**, 1871-1873.

57. Askounis A, Orejon D, Koutsos V, Sefiane K, Shanahan M E. Nanoparticle deposits near the contact line of pinned volatile droplets: size and shape revealed by atomic force microscopy. Soft Matter, 2011, 7, 4152-4155.

58. Lee S-J J. *Microfabrication for microfluidics*. Boston: Artech House: Boston, 2010.

59. Kubyshkina V., Orejon D., Dover C.M., Sefiane K., Geometrical Deposits on Microstructured Surfaces, Journal of Bionic Engineering, 2020, 17, 851-865.

60. de Gennes P-G, Brochard-Wyart F, Quéré D. *Capillarity and Wetting Phenomena.* Springer, New York, United States of America, 2004.

61. Crivoi A, Zhong X, Duan F. Crossover from the coffee-ring effect to the uniform deposit caused by irreversible cluster-cluster aggregation. *Physical Review E,* 2015, **92**, 032302.

62. Li Y, Yang Q, Li M, Song Y. Rate-dependent interface capture beyond the coffee-ring effect. *Scientific reports,* 2016, **6**, 1-8.

63. Hemalatha J, Prabhakaran T, Pratibha Nalini R. A comparative study on particle–fluid interactions in micro and nanofluids of aluminium oxide. *Microfluidics and Nanofluidics,* 2011, **10**, 263-270.